On the Use of Refractive Index Diagrams for Source-Excited Anisotropic Regions*

Leopold B. Felsen

Contribution From the Department of Electrophysics, Polytechnic Institute of Brooklyn, Brooklyn, N.Y.

The use of refractive index diagrams in the study of plane wave propagation in unbounded and layered anisotropic media is reviewed and then extended to account for certain aspects of the radiation from confined source distributions. Such items as the radiation condition, saddle point location, focusing effects, lateral ray trajectories, Cerenkov radiation, and others are interpreted via the refractive index plots. While some of this material is available in various technical publications, the aim here is at a more unified presentation.

1. Introduction

Since the problem of propagation of plane waves in a wholly or piecewise homogeneous anisotropic medium already involves considerable complexity, it may be anticipated that the difficulties are compounded further when spatially confined sources are present. The thorough understanding of the behavior of plane waves is an essential prerequisite since the fields caused by localized distributions of sources may be synthesized by plane wave superposition. While the entire wave spectrum is required for a detailed description at any point in space, the field at observation points "far" from the source region, where a few propagating plane waves suffice to describe the essential features of the local field structure, may be characterized in a much simpler form. In analytical terms, the distant field is found from an asymptotic evaluation of the exact plane wave integral representation, the major contribution to which arises from the stationary points in the integrand. Each of the stationary points selects a particular plane wave which then appears in the asymptotic approximation. It may be surmised from these considerations that the selection of the appropriate waves appearing in the far field is a matter of basic concern.

While these observations apply also to the isotropic case, their resolution is trivial in this instance. Since all propagating plane waves $\sim \exp(i\mathbf{k} \cdot \mathbf{r})$ are characterized by the same wave number $k = k_0 n$, where k_0 is the wave number in vacuum and n is the (constant) refractive index in the medium, the field at a distant observation point P is furnished by that wave whose wave vector $\mathbf{k}$ is parallel to the radius vector from the source region to P. This situation no longer obtains in an anisotropic medium where k depends on the direction of propagation; it is also necessary to distinguish between the directions of phase propagation (given by $\mathbf{k}$) and power flow since these do not in general coincide. There arise

then some basic problems even about the determination of the contributing plane waves in the far field, apart from the specification of their amplitude and polarization.

Owing to the generally complicated functional dependence of k or n on the propagation angle [for the magneto-ionic medium, see Budden, 1961], it has been found useful to construct plots of these quantities which are termed wave vector and refractive index plots, respectively. From these diagrams, which have the form of multibranched surfaces, it is possible to ascertain the value of $\mathbf{k}$ and also the corresponding direction of power flow for any given spatial orientation. While refractive index surfaces have been employed for some time in connection with plane wave propagation, their use for radiation problems is of relatively recent origin. The latter aspect forms the motivation for this paper which begins with a review of some basic notions concerning the wave vector, group velocity and Poynting vector, and then proceeds to the study of radiation problems in an unbounded, homogeneous, lossless region. It is shown how the refractive index plot may be utilized for the imposition of the radiation condition on the exact integral representation; the determination of the stationary points in the integrand, and therefore the selection of the plane wave constituents in the far field as well as the delineation of their domains of existence (some waves may appear only in limited sections of space); and the specification of those spatial regions wherein field enhancements (focusing) may take place (these effects are not observed in isotropic configurations). The source configurations include point sources, line sources with and without progressive phase variation, highly directive distributions, and charges in uniform motion (Cerenkov effect). In all of these instances, the refractive index diagram furnishes in a simple and direct manner information about the frequently tortuous ray structure (trajectories of power flow) and grants an insight into the radiation mechanism (but not directly into the polarization or angular intensity variation of a given ray species). These considerations are then extended to account for the presence

of a plane interface and for such phenomena as non-specular reflections, focusing, and lateral waves. To avoid the use of usually complicated analytical formulas in justification of results deduced for anisotropic configurations, a reasonably detailed application of pertinent concepts is given first for the thoroughly familiar isotropic case wherein the surfaces have an especially simple shape. The extrapolation to the anisotropic regime should then be fairly evident. It should be mentioned that many of the aspects entering into the discussion have been noted variously in the literature to which reference is made; the principal aim in the present writing is at a unified presentation. Finally, while specific mention is made only of the magneto-ionic problem (single-species, zero temperature plasma), the same considerations apply also more generally [Lighthill, 1960].

2. Refractive Index Surface, Wave Vector, and Ray

A space-time dependent electromagnetic field in an unbounded homogeneous medium may be represented as a continuous superposition of plane waves which are characterized by a frequency ω and by a wave vector $\mathbf{k}=\mathbf{x}_0 k_x+\mathbf{y}_0 k_y+\mathbf{z}_0 k_z$. If the medium[1] may be characterized at a given frequency in terms of a tensor permittivity $\underset{\sim}{\epsilon}$ and a scalar permeability μ_0 (this applies, for example, to the magneto-ionic situation), each time-harmonic plane wave constituent descriptive of the electric field,

$$\mathbf{E}(\mathbf{r})=\mathbf{A}e^{i(\mathbf{k}\cdot\mathbf{r}-\omega t)}, \qquad (1)$$

must satisfy the vector wave equation,

$$\nabla\times\nabla\times\mathbf{E}-\frac{\omega^2}{c^2}\underset{\sim}{\epsilon}'\cdot\mathbf{E}=0, \qquad \underset{\sim}{\epsilon}'=\frac{\underset{\sim}{\epsilon}}{\epsilon_0}. \qquad (2)$$

$\mathbf{A}$ is a constant vector, c the propagation speed in vacuum, $\underset{\sim}{\epsilon}'$ the normalized permittivity, and $\mathbf{r}=\mathbf{x}_0 x+\mathbf{y}_0 y+\mathbf{z}_0 z$ the position vector. The magnetic field may be derived in terms of $\mathbf{E}$ from the Maxwell equations. The parameters $\mathbf{k}$ and ω in (1) are not independent but are connected by the *dispersion relation* obtained upon substituting (1) into (2) (note: $\nabla\rightarrow i\mathbf{k}$):

$$\det\underset{\sim}{Q}=0, \qquad \underset{\sim}{Q}=\mathbf{k}\times(\mathbf{k}\times\underset{\sim}{1})+\frac{\omega^2}{c^2}\underset{\sim}{\epsilon}', \qquad (3)$$

where the unit dyadic $\underset{\sim}{1}$ is defined so that $\underset{\sim}{1}\cdot\mathbf{A}=\mathbf{A}\cdot\underset{\sim}{1}=\mathbf{A}$. Since (3) makes possible the solution for one of the parameters k_x, k_y, k_z, ω in terms of the other three, there exist two essentially different ways of representing this dependence:

$$(a)\ \omega=\omega(k_x, k_y, k_z),\ \text{or}\ (b)\ k_z=k_z(k_x, k_y, \omega). \qquad (4)$$

In case (a), the frequency variable is regarded as a function of the wave vector $\mathbf{k}$ whereas in (b), one of the wave numbers, k_z, is a function of the remaining wave numbers k_x, k_y, and of ω. The representation of the space-time dependent field $\hat{\mathbf{E}}(\mathbf{r}, t)$ via case (a) involves a triple Fourier integral in $\mathbf{k}$-space [Ginzburg, 1960; Stix, 1962]

$$\hat{\mathbf{E}}(\mathbf{r}, t)=\int_{-\infty}^{\infty}dk_x\int_{-\infty}^{\infty}dk_y\int_{-\infty}^{\infty}dk_z\bar{\mathbf{A}}(\mathbf{k})e^{i[\mathbf{k}\cdot\mathbf{r}-\omega(\mathbf{k})t]}, \qquad (5a)$$

while the one in case (b) leads to a representation in terms of "guided waves" along z [Budden, 1961],

$$\hat{\mathbf{E}}(\mathbf{r}, t)=\int_{-\infty}^{\infty}d\omega\int_{-\infty}^{\infty}dk_x$$
$$\int_{-\infty}^{\infty}dk_y\mathbf{A}(\mathbf{k}_t, \omega)e^{i[\mathbf{k}_t\cdot\boldsymbol{\rho}-\omega't+k_z(\mathbf{k}_t, \omega)z]}, \qquad (5b)$$

with $\mathbf{k}_t=\mathbf{k}-\mathbf{z}_0 k_z$, $\boldsymbol{\rho}=\mathbf{r}-\mathbf{z}_0 z$. These integrations must be carried out separately for all possible solutions $\omega(\mathbf{k})$ or $k_z(\mathbf{k}_t, \omega)$.

The representations (5a) and (5b) are useful for different purposes. Energy transport properties of a quasi-monochromatic signal, expressed in terms of the group velocity vector $\mathbf{v}_g$, are readily deduced from (5a). In this instance, $\mathbf{A}(\mathbf{k})$ has a sharp peak at a wave number k' corresponding to $\omega_0\equiv\omega(k')$, and the signal $\hat{\mathbf{E}}(\mathbf{r}, t)$ is a maximum along trajectories defined by the stationary phase points of the integrand for which the individual plane waves interfere constructively:

$$\nabla_k\varphi(\mathbf{k})=0\ \text{at}\ k', \qquad \varphi(\mathbf{k})=\mathbf{k}\cdot\mathbf{r}-\omega(\mathbf{k})t, \qquad (6)$$

with $\nabla_k\equiv\mathbf{x}_0(\partial/\partial k_x)+\mathbf{y}_0(\partial/\partial k_y)+\mathbf{z}_0(\partial/\partial k_z)$ denoting the gradient operator in k-space. With $\mathbf{v}_g\equiv\mathbf{r}/t$ along the trajectory, one finds from (6) that

$$\mathbf{v}_g=\nabla_k\omega. \qquad (7)$$

The direction of energy flow, parallel to $\mathbf{v}_g$, is called the "ray direction" and differs in general in an anisotropic medium from that of the wave vector $\mathbf{k}$ which is perpendicular to the equiphase surface $\varphi=$constant. It is in fact evident from (7) that $\mathbf{v}_g$ is perpendicular to the surface $\omega(\mathbf{k})=$constant, i.e., to the constant frequency surface descriptive of the solution of the dispersion equation (3). Via (4b), the equation $k_z=k_z(k_x, k_y; \omega)$ describes for a fixed ω a surface which contains the endpoints of the wave vector $k\equiv|\mathbf{k}|$, and this plot in k-space is normalized conveniently by introduction of the refractive index $n(k_x, k_y; \omega)$:

$$k=\frac{\omega}{c}n. \qquad (8)$$

Apart from the normalization factor $k_0=\omega/c$, the wave vector and refractive index diagrams evidently

---

[1] To simplify the discussion, the medium is assumed to be lossless.

contain the same information at a specified frequency. Since the group velocity vector $\mathbf{v}_g$ (or the ray vector) for an essentially monochromatic plane wave has been shown to be perpendicular to the refractive index surface, it follows that $\mathbf{k}$ and $\mathbf{v}_g$ are parallel everywhere only when $|\mathbf{k}|$ is independent of direction, i.e., when the surface is a sphere. This obtains in an isotropic, but not in an anisotropic, region. In what follows, we shall be concerned almost exclusively with solutions of the dispersion equation which yield real values of k_x, k_y, k_z corresponding to propagating plane waves in (1); while nonreal k_z may arise in (5b) in view of the infinite range of k_x, k_y (see sec. 3.1), these evanescent fields do not carry energy away from the source region. It may be noted that monochromatic processes are described conveniently in terms of (5b) since the ω-integration is then absent (the ω-dependence of $A(\mathbf{k}_t, \omega)$ is in the form $\delta(\omega-\omega_0)$, where ω_0 is the operating frequency). Even these simple considerations illustrate the utility of one or the other formulations in (4) and (5).

For an explicit evaluation of the group velocity in terms of the refractive index $n(k; \omega)$, it is convenient to proceed from the implicit differentiation formula

$$\frac{\partial f}{\partial k_i} + \frac{\partial f}{\partial \omega}\frac{\partial \omega}{\partial k_i} = 0, \qquad i = x, y, z, \qquad (9)$$

applied to $f(k; \omega) \equiv k - n\omega/c = 0$, which may then be solved for the components $(\partial\omega/\partial k_i)$ of $\mathbf{v}_g$. If the k-surface is rotationally symmetric about one of the axes, say k_z (this corresponds in the magneto-ionic case to an applied steady magnetic field parallel to z), it is convenient to define the polar angle $\bar{\theta}$ via $\sin \bar{\theta} = k_\rho/k$, $\cos \bar{\theta} = k_z/k$, and one may verify without difficulty that [Ginzburg, 1960; Budden, 1961; Stix, 1962]

$$v_g = \frac{c}{\cos \alpha \dfrac{\partial}{\partial \omega}(n\omega)}, \quad v_{gk} = r_g \cos \alpha, \ v_{g\bar{\theta}} = v_g \sin \alpha,$$
$$(9a)$$

where

$$\tan \alpha = \frac{\partial n}{n \partial \bar{\theta}}. \qquad (9b)$$

In these expressions, $n(\theta; \omega)$ is regarded as a function of $\bar{\theta}$ and ω, v_{gk} and $v_{g\bar{\theta}}$ are the components of $\mathbf{v}_g$ along and perpendicular to the wave vector $\mathbf{k}$, respectively, and α is the angle between $\mathbf{v}_g$ and $\mathbf{k}$. One may show that $|\alpha| < \pi/2$—an observation important for the imposition of a radiation condition for problems involving confined source distributions in a magneto-ionic medium. Equation (9b) confirms that $\mathbf{v}_g$ is perpendicular to the $n(\bar{\theta})$ surface.

It is also of interest to state a simple relation between the group velocity $\mathbf{v}_g$ and the time-averaged Poynting vector $\mathbf{S} \equiv \text{Re }(\mathbf{E} \times \mathbf{H}^*)$ for a monochromatic plane wave propagating in a lossless, dispersive, anisotropic medium:

$$\mathbf{S} = W\mathbf{v}_g, \qquad (10)$$

where W is the average stored energy density,

$$W = \frac{1}{2}\left\{ \mathbf{E}^* \cdot \frac{\partial}{\partial \omega}[\omega\boldsymbol{\varepsilon}(\omega)] \cdot \mathbf{E} + \mu_0|\mathbf{H}|^2 \right\}. \qquad (10a)$$

While certain aspects of (10) for the magneto-ionic medium may be verified by direct but tedious calculation [Hines, 1951; Abraham, 1953], its validity may be confirmed from a more basic and elegant analysis [Stix, 1962], the details of which are not presented here. The importance of (10) stems from the recognition that the ray direction in a lossless medium may be calculated either from $\mathbf{S}$ or $\mathbf{v}_g$, with the former often the more convenient once the field evaluation has been completed. Evidently, the vector $\mathbf{S}$ is also perpendicular to the $n(\bar{\theta})$ surface.

It should be clear from the preceding discussion that the refractive index diagram contains pertinent information required for the determination of the energy flow characteristics in a monochromatic plane wave characterized by a given wave vector $\mathbf{k}$. While the considerations so far have been restricted to an unbounded homogeneous medium, the refractive index plots may also be utilized effectively to ascertain the directions of the reflected and refracted rays at a plane interface between two media with different properties [Budden, 1961; see also sec. 5.3]. By partitioning a slowly varying medium into a sequence of homogeneous layers, one may in this manner chart the progress of a continuously refracted ray—a procedure which has found application in ionospheric propagation theory. It is the purpose in the remainder of this presentation to show how the refractive index plots may be used to advantage in predicting salient radiation characteristics of *confined source distributions* in unbounded and bounded anisotropic regions. As mentioned in the introduction, the pertinence of the preceding analysis stems from the fact that the fields due to spatially confined excitation, when observed at some distance, behave locally like plane waves. It may be noted that other plots (for example, of the ray velocity $c(n \cos \alpha)^{-1}$, or the ray refractive index $(n \cos \alpha)$) may be employed to schematize wave propagation characteristics in an anisotropic medium. However, the refractive index plot is the most pertinent to the analysis of integrals as in (5b) since it utilizes the k-space directly.

3. Spatially Localized Source Distributions in Unbounded Anisotropic Regions

The relevance of the foregoing remarks to radiation problems may be explored by referring to the integral (5b) which, upon omission of the ω-integration, represents in terms of a superposition of the previously described plane waves the response $\mathbf{E}(\mathbf{r})$ due to non-moving, arbitrarily prescribed time-harmonic sources

(the time factor exp $(-i\omega t)$ has been suppressed):

$$\mathbf{E}(\mathbf{r}) = \int_{-\infty}^{\infty} dk_x \int_{-\infty}^{\infty} dk_y \mathbf{A}(k_x, k_y) e^{i[k_x x + k_y y + k_z(k_x, k_y)z]}.$$

(11)

It is recalled that a separate integration is required for each of the relevant possible solutions $k_z(k_x, k_y)$ of the dispersion equation.
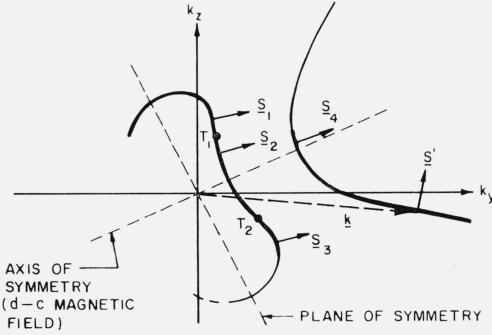

FIGURE 1. *Typical wave vector plot in* $\mathbf{k}_y, \mathbf{k}_z$-*plane.*

$T_{1,2}$—points of inflection.
Dark portion—satisfies radiation condition for $z > 0$.
Light portion—satisfies radiation condition for $z < 0$.

3.1. Radiation Condition

The function k_z (and $\mathbf{A}$ which generally depends on k_z) is multivalued in the k_x, k_y variables so that its definition is essential for the unique specification of the radiation integral (11). If the refractive index surface (or the wave vector surface $k = k_0 n$) is of finite extent (closed surface), k_z will be nonreal for sufficiently large (k_x, k_y). Let us suppose that the excitation is in the form of a point source located at $\mathbf{r} = 0$, in terms of which any distributed driving function may be synthesized. Convergence of the integral then requires that Im $k_z \gtrless 0$ for $z \gtrless 0$. Physically, this radiation condition implies that the nonpropagating wave fields decay away from the source region. If the medium contains some losses so that k_z has an imaginary part for all (k_x, k_y), the above-stated condition suffices to define k_z everywhere and assures the vanishing of the field at $\mathbf{r} \rightarrow \infty$. In analytical terms, the branch point singularities of k_z are then displaced from the real k_x, k_y axes, thereby making the integrand unambiguous along the entire integration path.

To effect a definition of k_z when this function is real, one may approach the limit of vanishing dissipation from the above-mentioned lossy case, and the required distortion of the integration path as the branch point singularities of k_z approach the real axis is then made evident. This distortion of the path is equivalent to effecting the consistent definition of the multivalued function k_z for complex and real values. Alternatively, and frequently more conveniently, the proper definition of k_z, when real,

may be achieved directly from the refractive index plot [Arbel and Felsen, 1963]. Since the radiation condition requires that each constituent propagating plane wave transport energy away from the source region,[2] the permissible portion of the refractive index surface for $z > 0$ is that for which the surface normals have a component in the $+z$-direction; it is important to recall in this connection that the sense of the normal is such as to make its angle with the wave vector $\mathbf{k}$ less than 90° (see fig. 1, where a section through the k_y, k_z plane is shown). The converse argument applies when the observation point lies in $z < 0$. Having thus identified the appropriate branches of the refractive index plot, one may determine by inspection the correct algebraic sign of k_z. As noted from figure 1, it may happen that $k_z < 0$ when $z > 0$ (rays $\mathbf{S}'$ or $\mathbf{S}_3$), thereby leading to a phase progression along $(-z)$ while energy advances along $(+z)$. This corresponds to a "backward wave" with respect to the z-axis, a common occurrence in anisotropic media [see also Clemmow, 1963].

If the refractive index surface has an open branch so that k_z is real for all values of k_x and (or) k_y, the preceding arguments may be applied as well. The integral (11) is then no longer exponentially convergent, and the field may grow without limit in certain spatial directions. This aspect is explored further in section 3.3b.

3.2. Saddle Point Condition

To effect a reduction of the integral (11), it is noted that the far fields are contributed essentially by those area elements in the k_x, k_y-plane surrounding the stationary points in the exponent. The stationary phase condition

$$\frac{x}{z} = -\frac{\partial k_z}{\partial k_x}, \quad \frac{y}{z} = -\frac{\partial k_z}{\partial k_y},$$

(12)

selects those values of k_x and k_y for which the normal to the refractive index surface points in the direction from the origin in the source region to the distant observation point, $\mathbf{r}$. Since the normal to the surface has been seen to specify the direction of power flow, one recognizes that the major contribution to the far field arises precisely from those plane waves (rays) which carry energy from the source to the observation point along a straight line trajectory. Conversely, the refractive index plot may be utilized to determine the real stationary (saddle) points in the k_x, k_y wave number space: one finds all points on the surface having a normal parallel to the prescribed radius vector $\mathbf{r}$ (see for example the four rays $\mathbf{S}_1 \ldots \mathbf{S}_4$ in fig. 1), and reads off the corresponding values of k_x, k_y which

[2] The radiation condition, which requires the outward flow of total energy, must be satisfied for arbitrary source configurations, i.e., arbitrary $\mathbf{A}$ in (11). One then concludes that each plane wave constituent must individually satisfy this condition [see Arbel and Felsen, 1963].

locate the saddle points, remembering the previously mentioned radiation condition that the angle between **k** and the ray is less than 90°. These graphical considerations therefore aid substantially in the visualization of the saddle point configuration pertaining to the integral (11) [Lighthill, 1960; Arbel and Felsen, 1963; Mittra and Deschamps, 1963; Kogelnik and Motz, 1963].

3.3. Ray Amplitudes

a. Curvature of Refractive Index Surface

The refractive index plots furnish information not only about the multiplicity and propagation characteristics of the rays reaching a distant observation point, but also about the ray amplitudes. The asymptotic evaluation of the double integral (11) may be carried out by adding the contributions from the vicinity of all appropriate stationary points satisfying condition (12). Since the choice of coordinate axes with respect to the dispersion surface has been left arbitrary, we may select an orientation so that the z-axis is parallel to the radius vector **r**; i.e., $x=y=0$ in (11), and the saddle points are defined by those points on the surface with normal parallel to z. In the vicinity of a saddle point $(k_{xj}, k_{yj}) \equiv \mathbf{k}_{tj}$, the presumedly slowly varying function **A** may be approximated by $\mathbf{A}(k_{xj}, k_{yj}) \equiv \mathbf{A}_j$, and the function k_z in the exponential may be represented by the first few terms in its power series expansion about (k_{xj}, k_{yj}). In view of (12), with $y=z=0$, the linear terms in $(k_x-k_{xj}) \equiv \xi$ and $(k_y-k_{yj}) \equiv \eta$ are absent. By orienting the (k_x, k_y) coordinates so that they coincide with the principal directions of curvature of the surface at the saddle point, one eliminates the $\xi\eta$-term and may write to terms of second order,

$$k_z(k_x, k_y) = k_{zj} + \tfrac{1}{2}K_{xj}\xi^2 + \tfrac{1}{2}K_{yj}\eta^2 + \ldots, \quad (13)$$

with $K_{xj} = \partial^2 k_z/\partial k_x^2]_j$ and $K_{yj} = \partial^2 k_z/\partial k_y^2]_j$ representing the associated curvatures, and $k_{zj} \equiv k_z(k_{xj}, k_{yj})$. Thus, the asymptotic approximation of **E**(**r**) for large values of z is given by [Lighthill, 1960]:

$$\mathbf{E}(\mathbf{r}) \sim \sum_j \mathbf{A}_j e^{ik_{zj}z} \int_{-\infty}^{\infty} e^{izK_{xj}\xi^2/2}d\xi \int_{-\infty}^{\infty} e^{izK_{yj}\eta^2/2}d\eta \quad (14a)$$

$$= \frac{2\pi}{z} \sum \mathbf{A}_j e^{ik_{zj}z} \frac{e^{i[\text{sgn}\,K_{xj}+\text{sgn}\,K_{yj}]\pi/4}}{\sqrt{|K_j|}} + O\left(\frac{1}{z^2}\right), \quad (14b)$$

where $K_j \equiv K_{xj}K_{yj}$ is the Gaussian curvature at the jth contributing saddle point included in the sum. The detailed structure of $\mathbf{A}_j$ depends both on the medium parameters (i.e., the refractive index profile) and on the nature of the source configuration. While the preceding considerations yield *all* the possible rays which may propagate from the source to the observation point, it should be kept in mind that specific source configurations may excite only some of these.

Equation (14b) states that the distant field radiated by a confined source distribution is comprised of radial rays along which the field decays according to $(1/r)$. The angular pattern (i.e., the amplitude) of the field along a given ray is governed by the coefficient $\mathbf{A}_j$ which is generally well behaved, and by the factor $K_j^{-1/2}$. Disregarding $\mathbf{A}_j$, the amplitude evidently increases when the ray originates from a "slowly curved" segment of the dispersion surface, and it appears to grow without bound when one of the principal radii of curvature vanishes. A closer investigation of the refractive index plot reveals that $K_j \to 0$ implies the coalescence of two saddle points and therefore the strong interaction of two almost identical ray species (see fig. 1, where $k_{y1} \to k_{y2}$ when the radius vector **r** from the source to the observation point becomes perpendicular to the curve at the inflection point T_1; similar considerations apply to T_2). This situation requires a modification of the asymptotic evaluation of (11) wherein it was assumed that the saddle points are simple $(K_{xj}, K_{yj} \neq 0)$ and separated. The calculation when $K_j \to 0$ leads to a radial dependence involving Airy functions and to field strengths enhanced over the $(1/r)$ dependence; details have been given elsewhere [Arbel and Felsen, 1963] and will not be repeated here. We should merely like to emphasize in the context of the present discussion that the occurrence of field enhancement by virtue of the interaction of rays arising from two adjacent stationary points may be predicted directly from the presence of points of inflection in the refractive index diagram.

b. Open Branches of Refractive Index Surface

If the refractive index surface contains unbounded branches, there will exist certain ray directions corresponding to saddle points $k_{xj} \to \infty$ and (or) $k_{yj} \to \infty$. Since k_z is now real over the entire integration interval, the integral (11) is no longer exponentially convergent, and **E**(**r**) may actually diverge when the saddle point moves to infinity. The nature of the singularity depends on the source configuration; it is most pronounced for point source excitation but may actually be made to disappear for sufficiently smooth source distributions. Details of the analysis are available elsewhere [Arbel and Felsen, 1963; Felsen, 1964a] and it suffices for the present to note that the singular ray directions may be inferred easily from the refractive index diagram (see ray **S**′ in fig. 1, as $k \to \infty$ along the open branch; the singular ray direction is perpendicular to the asymptote).

3.4. Domain of Existence of a Particular Ray Species

If the refractive index surface possesses undulations ("bumps" or "dimples") or unbounded branches, not all regions of space are illuminated by the same ray species. For example, if θ_1 and θ_2 denote the angles between the positive k_z-axis and the normals at T_1 and T_2, respectively, in figure 1, ray **S**$_1$ reaches those observation points in the first quadrant of the y, z plane whose angular deviation θ from the z-axis lies in the interval $0 \leq \theta \leq \theta_1$. Ray **S**$_2$ is confined to $\theta_2 \leq \theta \leq \theta_1$, ray **S**$_3$ exists in $\theta_2 \leq \theta \leq \pi/2$, and ray

S_4 in $\theta_3 \leq \theta \leq \pi/2$ with θ_3 representing the inclination of the normal to the asymptote of the open branch. The angular domain wherein a ray species exists is its zone of illumination and the remaining region is the shadow zone wherein the fields on the ray in question are exponentially small. It is evident that the zones of illumination and shadow may be inferred directly from the refractive index plot from which it is seen, for example, that rays S_1 and S_2 are absent when $\theta_1 \leq \theta \leq \pi/2$ (the corresponding saddle points are complex in this range) while the shadow region for rays S_2 and S_3 is $0 \leq \theta < \theta_2$ (see also fig. 8).

4. Source Problems in Isotropic Regions

To illustrate specific application of the preceding concepts in their simplest form, a number of radiation problems in isotropic configurations are reviewed and interpreted via the refractive index plots. In a homogeneous isotropic medium, $\overline{\epsilon} = 1\epsilon$, and one obtains from (3) the dispersion relation

$$k = \frac{\omega}{c}\sqrt{\epsilon'} = k_0 n, \quad k = \sqrt{k_x^2 + k_y^2 + k_z^2} = \sqrt{k_t^2 + k_z^2},$$

where n may depend on ω but not on $\overline{\theta}$. As noted previously, the refractive index plot reduces to a sphere in this instance so that the directions of the wave vector $\mathbf{k}$ and the ray $\mathbf{S}$ coincide.

4.1. Sources in an Unbounded Region

a. Point Source

The fields radiated by an arbitrarily oriented electric or magnetic current element in an infinite, homogeneous, isotropic dielectric may be derived by suitable vector operations from the scalar Green's function

$$G = \frac{e^{ikr}}{4\pi r}, \tag{15a}$$

which has the integral representation

$$G = \frac{i}{8\pi^2} \int_{-\infty}^{\infty} dk_x \int_{-\infty}^{\infty} dk_y \, \frac{e^{i[k_x x + k_y y + k_z|z|]}}{k_z},$$

$$k_z = \sqrt{k_0^2 n^2 - k_x^2 - k_y^2}. \tag{15b}$$

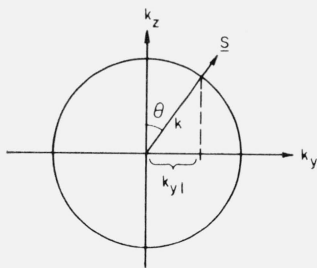

FIGURE 2. *Wave vector surface for isotropic medium:* $\mathrm{k} = \mathrm{k_0 n}$.
Saddle point—$k_{y1} = k \sin \theta$.

(The above-mentioned vector operations account for the detailed structure of $\mathbf{A}$ in (11) for different source configurations.) While the solution for this trivial example is known in the closed form (15a), the integral (15b) shall be investigated per se for purposes of illustration.

Because of the spherical symmetry, the coordinate system may be chosen so that $x = 0$, thereby leading to the diagram in figure 2. In view of the dependence on $|z|$ in (15b), only the region $z > 0$ need be considered. k_z must be positive imaginary when non-real, and it is evident from the diagram in figure 2 that to satisfy the radiation condition, k_z is positive when real. It follows from this definition that the integration path is indented into the lower and upper halves of the k_x plane to avoid the branch points at $k_x = \sqrt{k_0^2 n^2 - k_y^2}$ and at $k_x = -\sqrt{k_0^2 n^2 - k_y^2}$, respectively, when $k_y^2 < k_0^2 n^2$. Analogous considerations apply to the k_y-integration. The same conclusions are reached when dissipation is assumed initially (Im $n > 0$) and the lossless case is approached subsequently. One observes, incidentally, that the branch points correspond to those portions of the refractive index surface for which the associated rays are confined to the $z = 0$ plane (separation between rays going into $z > 0$ and $z < 0$, respectively); this latter observation holds also under more general circumstances where these singularities are no longer defined by the simple condition $k_z = 0$.

From the discussion in section 3.2 and figure 2, it follows that the only saddle point of the integrand in (15b) (with $x = 0$) is located at $k_{y1} = k \sin \theta$, where $\theta = \tan^{-1}(y/z)$ specifies the angular location of the observation point. While this conclusion is reached at once from the geometrical construction, it may of course be verified from (12) by direct calculation. Each distant observation point is therefore reached by a single radial ray with wave vector k.

Since the principal curvatures of the spherical surface are constant and equal to $(-1/k)$, one obtains directly from (14b) that the asymptotic approximation to G is given by the expression (15a) (which in this instance happens to hold for all r). None of the complicating features due to points of inflection or open branches of the refractive index surface arise here. It should be recalled that the angular variation of the ray amplitude also depends on the nature of the source and emerges from the derivation of the field via the scalar Green's function G.

b. Line Source

Constant phase. If the excitation is in the form of electric and (or) magnetic currents distributed uniformly along a line, say the y-axis, then the entire field structure is independent of the y-coordinate, and the constituent plane waves descriptive of this field configuration must be characterized by $k_y = 0$. Consequently, the effective portion of the refractive index diagram is the curve formed

by the intersection of the sphere in figure 2 with the plane $k_y=0$. The corresponding surface normals are confined to the x, z-plane so that energy leaves the source along radial rays which lie in a plane perpendicular to the source axis. The polarization of the field, or its angular intensity distribution, depends, of course, on the details of the source configuration.

Linearly progressing phase. If there is impressed on the previously mentioned line distribution a phase variation $\exp (ik_{y1}y)$, where k_{y1} is a real constant, then the resulting fields in this y-invariant structure must exhibit the same y-dependence. The constituent plane waves are therefore characterized by $k_y=k_{y1}$, which requirement reduces the double integral in (11) to a single one over k_x (the k_y-dependence of $\mathbf{A}(k_x, k_y)$ is in the form $\delta(k_y-k_{y1})$). The radiation characteristics are now inferred from the intersection of the plane $k_y=k_{y1}$ with the refractive index surface in figure 2. One observes that if $|k_{y1}|<k$, energy emanates from the source along rays which lie on a circular cone having an apex angle $\psi=\cos^{-1} (k_{y1}/k)$ with respect to the source axis (fig. 3). It is evident from figure 2 that real rays exist only when $|k_{y1}|<k$. For $|k_{y1}|>k$, there is no real solution for k_z and radiation does not occur. The intervals $|k_{y1}|<k$ and $|k_{y1}|>k$ distinguish phase velocities along the source distribution which are larger and smaller, respectively, than the velocity of light in the medium; as is well known, the former wave types radiate whereas the energy in the latter is bound to the source region.

The validity of the preceding remarks is easily verified from the scalar Green's function

$$G=\frac{i}{4} e^{ik_{y1}y} H_0^{(1)} [\sqrt{(k^2-k_{y1}^2)(x^2+z^2)}] \tag{16a}$$

$$=\frac{i}{4\pi} e^{ik_{y1}y} \int_{-\infty}^{\infty} \frac{e^{ik_x x+k_z|z|}}{k_z} dk_x, \ k_z=\sqrt{k^2-k_x^2-k_{y1}^2}, \tag{16b}$$

in terms of which the electromagnetic fields may be derived. For example, if the source is a line of electric currents of unit strength, then the nonvanishing field components are

$$E_y=\frac{1}{i\omega\epsilon}\left(\frac{\partial^2}{\partial x^2}+\frac{\partial^2}{\partial z^2}\right)G, \ E_R=\frac{i}{\omega\epsilon}\frac{\partial^2 G}{\partial R \partial y}, \ H_\phi=-\frac{\partial G}{\partial R}, \tag{16c}$$

with $R=\sqrt{x^2+z^2}$ and $\phi=\tan^{-1} (z/x)$ denoting polar coordinates in the plane transverse to y. Using the asymptotic approximation of G, one finds $\mathbf{E} \sim (\boldsymbol{\nu}\times\boldsymbol{\phi}_0)k (k^2-k_{y1}^2)^{-1/2}E_y$, $\mathbf{H}\sim\sqrt{\epsilon/\mu}\boldsymbol{\nu}x\mathbf{E}$, where $\boldsymbol{\nu}$ is a unit vector along one of the rays sketched in figure 3. The Poynting vector is therefore parallel to $\boldsymbol{\nu}$. For $k_{y1}=0$, one recovers the case described in the first paragraph.
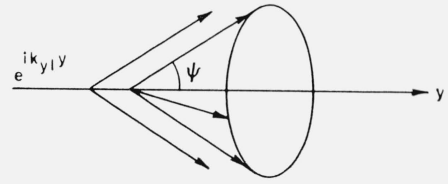

FIGURE 3. *Ray configuration for phased line source.*

c. Two-Dimensional Source Distribution

If the sources are distributed continuously over the entire x,y-plane with impressed phase variation $\exp (ik_{x1}x) \exp (ik_{y1}y)$, where k_{x1} and k_{y1} are real constants, then the field is described by a single plane wave with (k_{x1}, k_{y1}). The direction of energy flow is again inferred from that of the normal to the refractive index surface at this point. It is noted that radiation takes place only if $k_{x1}^2+k_{y1}^2<k^2$.

d. Highly Directive, but Confined, Source Distributions

The preceding phased one- and two-dimensional source distributions of infinite extent are idealizations which may, however, serve as approximations to large phased arrays or apertures of finite extent. Consider, for example, a progressively phased line source as in figure 3, confined to the interval $-a< y<a$. The amplitude function $\mathbf{A}(k_x, k_y)$ in (11) now contains the factor $[\sin (k_y-k_{y1})a](k_y-k_{y1})^{-1}$, which has a sharp peak at $k_y=k_{y1}$ if the source region is many wavelengths long. While this behavior is less violent than the $\delta(k_y-k_{y1})$ corresponding to $a\rightarrow\infty$, it nevertheless selects the plane waves with $k_y=k_{y1}$ as those contributing to the major peak(s) in the radiation field. The previously determined rays therefore point in the direction of the major lobes in the radiation pattern so that the refractive index diagram may be employed to find the locations of the radiated beam maxima.

e. Radiation From a Uniformly Moving Charge (Cerenkov Effect)

If a point charge q moves with constant velocity $\mathbf{v}$ along the y-direction, the associated electric current density $\hat{\mathbf{J}}$ may be characterized as follows:

$$\hat{\mathbf{J}}= \mathbf{y}_0 qv\delta(x-x')\delta(z-z')\delta(y-vt). \tag{17}$$

The frequency spectrum $\mathbf{J}$ of this source distribution is obtained by taking the temporal Fourier transform

$$\mathbf{J}=\frac{1}{2\pi}\int_{-\infty}^{\infty} e^{+i\omega t}\hat{\mathbf{J}}dt= \mathbf{y}_0\frac{q}{2\pi}\delta(x-x')\delta(z-z')e^{i(k_0/\beta)y}, \tag{18}$$

161

where $k_0 = \omega/c$ and $\beta = v/c$. This excitation for specified frequency corresponds precisely to the linearly phased line current discussed in section 4.1b, with amplitude $(q/2\pi)$ and impressed phase progression $k_{y1} = k_0/\beta$. The radiation characteristics at any given frequency may therefore be inferred from the results in section 4.1b, and the space-time dependent field is then recovered upon carrying out the ω-integration in (5b).

Since the particle speed is always less than the speed of light in vacuum, i.e., $\beta < 1$, one observes that $k_{y1} > k_0$. It is then obvious from figure 2 that no radiation will take place in vacuum for which the refractive index $n = 1$. In fact, radiation is possible only when the charge moves in a medium with refractive index $n > (1/\beta)$ for which one may satisfy the condition $k_{y1} < k$. If dispersion in the medium is neglected so that n is independent of frequency, then radiation at all frequencies will emerge along the well-known "Cerenkov angle"

$$\psi = \cos^{-1}\left(\frac{k_{y1}}{k}\right) = \cos^{-1}\left(\frac{1}{\beta n}\right), \qquad (19)$$

which may be determined graphically from the refractive index diagram (figs. 2 and 3). For a frequency dependent n, the Cerenkov angle will likewise be a function of frequency.

4.2. Influence of a Plane Boundary

In the preceding sections, the refractive index surface has been utilized for the determination of the power flow properties associated with various source distributions in unbounded media. The discussion is easily extended to accommodate the presence of a plane boundary which either terminates the region (for example, a perfect conductor) or separates it from another with different physical properties. The underlying analytical considerations are similar to those dealt with earlier. If it is assumed, for example, that the plane $z = 0$ separates two semi-infinite dielectrics with $n = n_1 (z < 0)$ and $n = n_2 (z > 0)$, then the fields of a z-directed point source located at $(0, 0, z')$, $z' < 0$, may again be derived from a scalar Green's function G which has a different representation in the two regions. In region 1 $(z < 0)$, G contains a direct and a reflected portion [Stratton, 1941]

$$G = G_1' + G_1'', \qquad (20)$$

$$G_1' = \frac{i}{8\pi^2} \int_{-\infty}^{\infty} dk_x \int_{-\infty}^{\infty} dk_y \frac{e^{i(k_x x + k_y y \pm k_{z1} z)}}{k_{z1}} e^{\mp ik_{z1} z'}, \qquad z \gtrless z' \qquad (20a)$$

$$G_1'' = \int_{-\infty}^{\infty} dk_x \int_{-\infty}^{\infty} dk_y \Gamma(k_x, k_y) \frac{e^{i(k_x x + k_y y - k_{z1} z)}}{k_{z1}} e^{-ik_{z1} z'}, \qquad (20b)$$

whereas in region 2 $(z > 0)$, the transmitted field is

derived from

$$G = G_2 = \int_{-\infty}^{\infty} dk_x \int_{-\infty}^{\infty} dk_y T(k_x, k_y) e^{i(k_x x + k_y y + k_{z2} z)} e^{-ik_{z1} z'},$$

$$k_{zi} = \sqrt{k_0^2 n_i^2 - k_x^2 - k_y^2}. \qquad (21)$$

Here, Γ and T represent the plane wave reflection and transmission coefficients, respectively, whose detailed form (for either E or H polarization) is readily evaluated but irrelevant to the present discussion. The important thing to be recognized is that the constituent plane waves in both regions are characterized by the *same* wave numbers k_x, k_y in the direction parallel to the interface—a condition required to assure continuity of the tangential field components across the boundary. The signs associated with k_{z1} and k_{z2} have been chosen in accord with the previously discussed radiation condition (sec. 4.1); in (20a), they assure the outward power flow from the source plane $z = z'$, in (20b) the flow of reflected power toward $z = -\infty$, and in (21) the flow of transmitted power toward $z = +\infty$.

a. Incident, Reflected and Refracted Rays

The familiar relation between the angles of incidence, reflection, and refraction of a plane wave, known as Snell's law, is inferred at once from the refractive index plots, a section of which is shown in figure 4. The propagating wave solutions corresponding to a given value $k_y = k_{y1}$ (with $k_x = 0$ through proper choice of coordinates) may be ascertained from figure 4 wherein it is assumed that $n_1 > n_2$. Evidently, four solutions are possible: two rays each progressing into $z > 0$ and $z < 0$, respectively. If a ray is incident on the interface from region 1 ($\mathbf{S}_1$), the corresponding reflected ray is $\mathbf{S}_1''$; since the surface $k = k_1$ is rotationally symmetric about the k_z-axis, the angles of incidence and reflection are equal (θ_1). Of the two ray solutions $\mathbf{S}_2$ and $\mathbf{S}_2''$ corresponding to the prescribed k_{y1} in region 2, $\mathbf{S}_2''$ must be discarded since it carries energy along the negative z-direction and therefore violates the radiation condition associated with an incident ray from below. The relation between the angles of
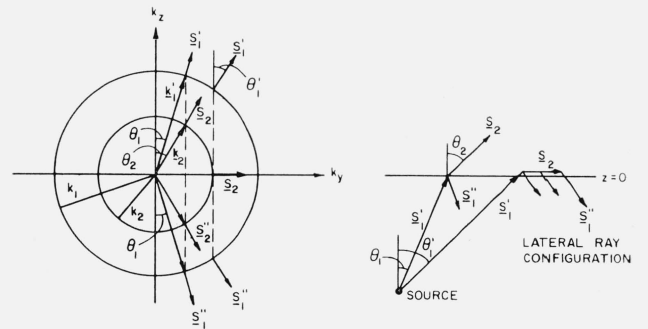

FIGURE 4. *Wave vector surfaces and rays for two different isotropic regions:* $k_i = k_0 n_i$.

refraction (θ_2) and incidence is obtained from the graph via the condition: $k_{y1}=k_1 \sin \theta_1=k_2 \sin \theta_2$, or $\sin \theta_2=(n_1/n_2) \sin \theta_1$ (Snell's law). Since the two surfaces are spherical, the incident, reflected and refracted rays all lie in a common plane. One notes that the k_2-branch is intersected only when $k_{y1}<k_2$; for $k_{y1}>k_2$, i.e., $\sin \theta_1>(n_2/n_1)$, k_{z2} is imaginary and no propagation takes place in region 2. The incident wave is then totally reflected.

b. Lateral Rays

When $k_{y1}=k_2$, the ray is incident at the critical angle $\theta_1'=\sin^{-1}(n_2/n_1)$ and the refracted ray proceeds parallel to the interface (see right-hand portion of fig. 4). This parallel ray, called a "lateral" ray, may refract back into region 1, thereby providing a mechanism for energy transfer which is entirely different from that associated with a reflected ray [Brekhovskikh, 1960]. In contrast to the discussion in section 4.2a which is relevant for an ordinary plane wave, the appearance of a lateral ray is connected intimately to the presence of a source of finite dimensions and owing to the continuous leakage of energy (see fig. 4), the amplitude of the field on a lateral ray is smaller than that on a reflected ray. While some further comments on this ray species are made later on, it is to be emphasized at this point that the existence and trajectory of a lateral ray may be inferred directly from the refractive index plot.

If the source is placed into the "thinner" dielectric (i.e., if $n_2>n_1$), the lateral ray is not excited since it is not possible to have $\theta_2=\pi/2$ for any incidence angle in the range $0\leq\theta_1\leq\pi/2$. The intimately related phenomenon of total reflection is also absent in this instance.

c. Asymptotic Evaluation of Reflected and Transmitted Fields

While the direct field G_1' may be evaluated as before (see (15a, b)), the reflected and transmitted fields require further attention. If we again set $x=0$ for convenience, the saddle point in the k_x integral is located at $k_{xs}=0$. The saddle point condition applied to the remaining integration in (20b) yields:

$$y+\frac{\partial k_{z1}}{\partial k_y}|z|+\frac{\partial k_{z1}}{\partial k_y}|z'|=0 \text{ at } k_{ys}. \qquad (22)$$

Since $(\partial k_{zi}/\partial k_y)=-\tan \theta_i$, where θ_i is the angle of the normal to the refractive index diagram at (k_{zi}, k_y), the straight line through (y, z) defined by (22) may be interpreted geometrically as follows: The observation point (y, z) in region 1 is reached via the ray trajectories $\mathbf{S}_1'$ and $\mathbf{S}_1''$ in such a manner that the angle of reflection is equal to the angle of incidence; this condition determines θ_1 and thereby the saddle point k_{ys} via figure 4. The equality of the angles of incidence and reflection follows from the symmetry of the refractive index plot; the ray interpretation of the saddle point condition is unaltered for more general situations where these angles may be different from one

another (see sec. 5.3). Confirmation of the ray interpretation in figure 5 is also had from the exponential in (20b) evaluated at the saddle point: $\exp[i(k_{ys}y+k_{z1}|z|+k_{z1}|z'|]$. Since $y=y_1+y_2$, the phase change is precisely the one required by a plane wave to travel from the source to the observation point via the ray trajectory $\mathbf{S}_1'$, $\mathbf{S}_1''$.

Analogous considerations apply to the evaluation of the transmitted field via (21). The saddle point condition now reads

$$y+\frac{\partial k_{z1}}{\partial k_y}|z'|+\frac{\partial k_{z2}}{\partial k_y}z=0 \text{ at } k_{ys}, \qquad (23)$$

and has a simple graphical interpretation: The observation point (y, z) in region 2 is reached via the ray trajectories $\mathbf{S}_1'$ and $\mathbf{S}_2$ in such a manner that the relation between the angles θ_1 and θ_2 is that specified by the refractive index plot in figure 4.

In summary, the saddle point determination required for the asymptotic evaluation of the reflected and transmitted fields, and the subsequent ray-optical interpretation of the result, may be carried out with the aid of the refractive index diagram: The source and observation points are connected by rays which satisfy the plane wave reflection or refraction laws, and the corresponding values of k_y yield the saddle points. From a knowledge of the saddle points, one may determine the ray amplitude via the remaining amplitude factor in the radiation integral.

The saddle points associated with propagating wave solutions in both regions are restricted to the interval $|k_{ys}|<k_1$ and $|k_{ys}|<k_2$ for the reflected and transmitted fields, respectively. If $k_1>k_2$, then the saddle points descriptive of the reflected field may cross the branch points at $\pm k_2$. Under these conditions, the asymptotic field contains another constituent arising from a branch point integration. This field type is the previously mentioned lateral wave whose existence and trajectory is readily predictable from the refractive index diagram. As noted from figure 4, the lateral wave contributes only when $\theta_1>\theta_1'$, thereby implying that the branch point contribution is absent when $|k_{ys}|<k_2$. This
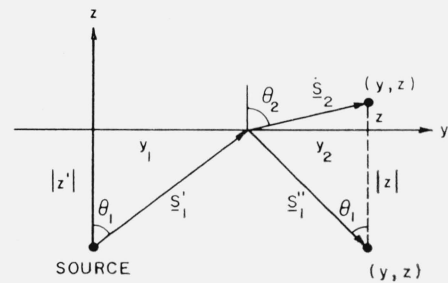

FIGURE 5. *Ray interpretation of saddle point condition for reflected and refracted fields* ($y_1+y_2=y$).
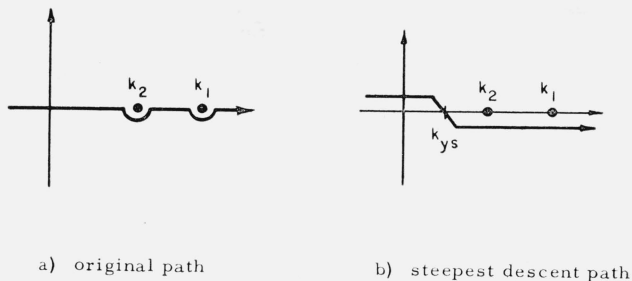
a) original path   b) steepest descent path

FIGURE 6. *Integration contours in complex* k_y*-plane.*
   a. Original path.
   b. Steepest descent path.

conclusion is confirmed from a study of the steepest descent path through the saddle point which involves a deformation of the integration contour away from the real axis, thus making unambiguous the domain of contribution from the branch point (see fig. 6).

d. Other Source Distributions

The preceding discussion has shown that the plane wave refractive index diagrams have direct application to the determination of the reflected or transmitted fields when a plane boundary is present. In essence, one first finds the ray structure in the unbounded region containing the source and then accounts for the interface by a ray-tracing procedure, with the trajectories of the reflected and transmitted rays ascertained from the diagram. With this in mind, the study of other source configurations is evident. For example, the highly directive sources described in section 4.1d excite strongly certain selected ray configurations whose characteristics in the presence of the interface are predicted from the refractive index plot. In this manner, one may find the directions of the reflected and transmitted beams. Cerenkov radiation due to a charge moving parallel to the boundary is also easily understood. If the charge moves in region 1 and $k_y = (k_0/\beta) < k_2 < k_1$, then radiation will occur in both regions at readily determined angles. For $k_1 > (k_0/\beta) > k_2$, propagation is possible only in region 1 and the energy is totally reflected at the interface, whereas for $(k_0/\beta) > k_1$, no radiation takes place. If the charge moves in region 2, radiation escapes into both regions when $(k_0/\beta) < k_2 < k_1$, but the fields in region 2 are evanescent when $k_1 > (k_0/\beta) > k_2$. Since propagation in region 1 is possible, however, under the latter condition, the incident evanescent fields may couple to propagating waves at the boundary.

4.3. Multiple and Gently Curved Interfaces

If the region is comprised of homogeneous layers (an inhomogeneous region may be so approximated), each layer has its own refractive index diagram and the previously described field matching procedure may be employed to chart the progress of a ray through the medium. The diagrams also reveal when a ray is "trapped" (ducting effect, bound waves): if a layer is bounded on both sides by media with smaller refractive index, it is possible to find wave solutions which propagate in the layer but decay outside.

In view of the ray interpretation of the fields radiated by confined source distributions, the ray tracing method may be applied locally even when an interface is nonplanar provided that the curvature is small over a length interval equal to the local wavelength [Keller, 1958]. Under these circumstances, the boundary at the point of impact of the ray is assumed plane, and the refractive index plots may then be used to determine the initial trajectories of the reflected and transmitted rays.

5. Further Discussion for Anisotropic Regions

The discussion in section 4 involving isotropic regions has served to illustrate the use of refractive index diagrams for the study of various familiar radiation problems. While the associated phenomena and their interpretation in terms of rays are in this simple case also easily deduced by other means, the refractive index plot offers distinct advantages in anisotropic regions where its contour may depart drastically from the spherical shape. With an understanding of the isotropic situation, one may proceed to apply the same considerations to the anisotropic case; the only difference is the substantially more complicated configurations of surfaces which depend on the form of the dielectric tensor $\boldsymbol{\epsilon}'$ in (3). For the magneto-ionic medium, they may be grouped into some eight categories [Clemmow and Mullaly, 1955; Allis, 1961; Deschamps and Weeks, 1962] which range from two concentric ovals to the undulating and open-branched configuration shown in figure 1, as the applied, cyclotron and plasma frequencies (for electrons) take on various values. The variety of surface contours is further increased when additional species (for example, ions) are taken into account in the description of a magneto-plasma [Allis, Buchsbaum, and Bers, 1962]. For the present discussion, the specific nature of the surfaces is of no concern and it suffices to deal with a typical case (as, for example, in fig. 1). It should of course be evident that the multibranched character of the refractive index plots implies the existence of more rays than those observed in the isotropic case. Even in the magneto-ionic medium wherein only electrons are considered mobile, as many as four different propagating solutions for $k_z(k_x, k_y)$ may be encountered. In view of the very complicated analytical expression for k_z in terms of k_x and k_y [Budden, 1961], it may be appreciated that much insight is gained from a plot of these quantities provided by the refractive index diagram.

The problem of radiation from a point source in an unbounded anisotropic region has already been dealt with in section 3. The anisotropy exerts in-

teresting effects also on other source distributions which are readily explored.

5.1. Line Source

The power flow characteristics for a uniform line source directed along the y-axis are inferred from the $k_y=0$ section through the refractive index plot. If the y-axis coincides with the direction of the axis of symmetry (gyrotropic axis), the normals to the surface in the $k_y=0$ plane are contained in this plane; the radiation therefore leaves the source in the radial direction and the rays are perpendicular to the line axis. For arbitrary inclination of the gyrotropic axis, however, the surface normals need not lie in the $k_y=0$ plane. With reference to figure 1, for example, the two rays with $k_x=0$, $k_y=0$ point into the first (top ray) and third (bottom ray) quadrants, respectively, with intermediate positions occupied by rays with $k_x \neq 0$. Energy thus travels along trajectories which are no longer perpendicular to the source axis although no phase variation is impressed along the source, a behavior in marked contrast to that observed earlier in the isotropic case. If the $k_y=0$ plane intercepts more than one branch of the refractive index surface, several ray species (with different orientation) may arise.

These observations apply also when the source possesses a progressive phase variation $\exp(ik_{y1}y)$, in which instance the intersection with the plane $k_y=k_{y1}$ is pertinent. For example, if k_{y1} is so large that only the open branch of the surface in figure 1 is intercepted, one obtains the ray structure shown in figure 7. In view of the requirement $\mathbf{k} \cdot \mathbf{S} > 0$, it
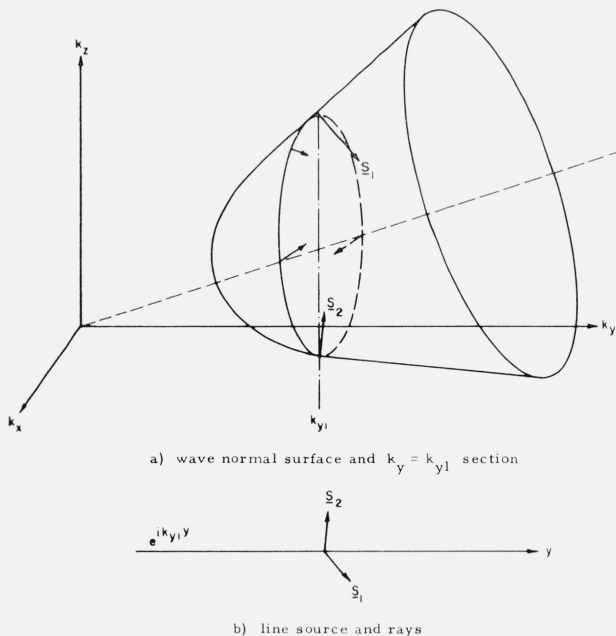
a) wave normal surface and $k_y = k_{y1}$ section

b) line source and rays

FIGURE 7. *Progressively phased line source inclined to gyrotropic axis (gyrotropic axis lies in y-z plane).*

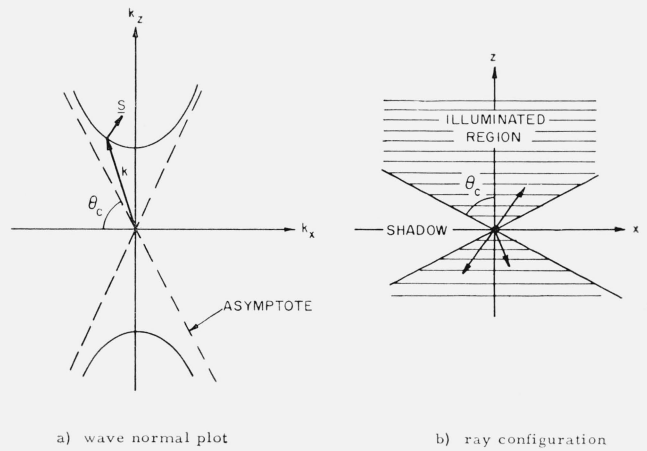a. Wave vector surface and $k_y=k_{y1}$ section.
b. Line source and rays.

a) wave normal plot

b) ray configuration

FIGURE 8. *Unphased line source perpendicular to gyrotropic axis.*

a. Wave vector plot.
b. Ray configuration.

is noted that the rays $\mathbf{S}_1$ and $\mathbf{S}_2$ in the $k_x=0$ plane are "backward" in the sense that the direction of phase progression is toward the source axis whereas energy necessarily flows outward. Evidently, the rays are not confined to a circular cone as in the isotropic problem (fig. 3).

Since the refractive index diagrams for the magneto-ionic medium are rotationally symmetric about the gyrotropic axis, substantial simplification in the ray picture results when the line source is oriented along, or perpendicular to, the axis of symmetry. In the former case, already mentioned earlier, the ray configuration is also rotationally symmetric and the rays in figure 7, for example, lie on a circular cone. In the latter instance, with $k_y=0$, the effective portion of the diagram comprises the plane section in the k_x, k_z plane as illustrated in figure 8 for the case of an open-branched surface. The rays are now confined to the x, z plane (i.e., they leave the source at right angles) and they illuminate only the shaded region in figure 8b).

5.2. Other Source Distributions

The preceding considerations concerning line distributions (and the analogous surface distributions described in section 4.1c) are again applicable to spatially confined but highly directive sources (see section 4.1d). For example, a planar phased array in the x–y plane with $k_x=0$, $k_y=k_{y1}$, produces two narrow beams which point asymmetrically along $\mathbf{S}_1$ and $\mathbf{S}_2$ in figure 7b, whereas a linear phased array with $k_y=k_{y1}$ produces beam maxima over a noncircular cone whose generators follow from figure 7 [Felsen and Rulf, 1963]. The result for the linearly phased line source (with $k_{y1}=k_0/\beta$ as in section 4.1d) may also be employed for the study of the radiation produced by a given spectral component at frequency ω arising from a point charge moving uniformly along the y-axis. Because of the

highly dispersive character of the magneto-ionic medium, the radiation characteristics differ greatly for various frequency ranges. Once the refractive index plots are available, it is a simple matter to ascertain when radiation may take place (i.e., when the Cerenkov "coherence condition" may be satisfied): one looks for possible intersections of the plane $k_y = (k_0/\beta)$ with the wave normal surface and infers the corresponding ray angles [Clemmow, 1963; McKenzie, 1963].

It must be emphasized that these graphical methods for the determination of major features in the power radiation pattern apply directly only when a single ray reaches a given observation point. If several rays are involved, their combined power pattern (which may deviate from the individual behavior) must be determined. It may happen, however, that the given source configuration excites one ray species more strongly than the others, in which instance the pattern is determined essentially by the most strongly excited ray.

5.3. Presence of a Plane Boundary

a. Ray Interpretation of Fields

If the gyrotropic medium is bounded by a plane interface at $z=0$, the radiation integral (11) must be augmented by additional contributions which account for the reflected and transmitted parts as in (20) and (21). Since there will generally be several solutions for $k_z(k_x, k_y)$ as evidenced by the multi-branched refractive index plots, it is understood that a separate integration is required for each pertinent k_z (corresponding, for example, to the ordinary and extraordinary modes). The resulting integrals are quite complicated [Barsukov, 1959; Arbel and Felsen, 1963; Tyras, Ishimaru, and Swarm, 1963] but as in the isotropic case (sec. 4.2), their detailed structure is of no concern here. We deal merely with the plane wave exponents in the integrands which may now have the more general structure

$$e^{i(k_x x + k_y y + k_{z1}^{(o,\ e)}|z| + k_{z1}^{(o,\ e)}|z'|)}$$

and

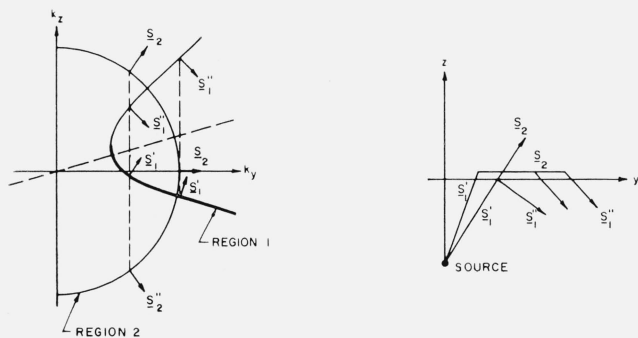$$e^{i(k_x x + k_y y + k_{z1}^{(o,\ e)}|z'| + k_{z2}z)}. \tag{24}$$

FIGURE 9. *Wave vector surfaces and rays for anisotropic and isotropic half-spaces.*

In this illustration for the magneto-ionic case, the superscripts o and e which denote the ordinary and extraordinary modes, respectively, may occur in any combination. The first exponential describes the reflected waves in region 1, with identical superscripts indicating reflection into the incident mode and different superscripts accounting for reflection into a different mode caused by coupling at the boundary. The second exponential describes the transmitted waves in region 2 which is assumed to be isotropic. If the boundary is perfectly reflecting so that no wave penetration into region 2 is possible, then integrals of the second type do not arise.

As in the isotropic case, the incident, reflected, and transmitted plane wave constituents are all characterized by the same transverse dependence on k_x, k_y, so that the wave vector plots may be used as before to chart the progress of the reflected and transmitted rays. As an illustration, consider the wave vector surface in figure 7 and assume that the anisotropic medium so described is separated from an isotropic dielectric half-space with refractive index n_2 by a plane interface at $z=0$ (the diagram implies that the gyrotropic axis is inclined with respect to the boundary). The composite plot (or rather its right half) descriptive of both regions is depicted in figure 9 wherein only the $k_x = 0$ plane is shown in order to simplify the drawing [Felsen, 1963]; the dark and light sections correspond to rays carrying energy along $+z$ and $-z$, respectively. The interpretation of figure 9 is directly analogous to that of figure 4 and the comments in sections 4.2a–4.2c need not be repeated here. It may be noted that although the incident, reflected and refracted rays lie in a single plane when $k_x = 0$, this condition does not obtain in the general case $k_x \neq 0$. Moreover, the angle of the reflected ray $\mathbf{S}_1''$ is not in general equal to the angle of the incident ray $\mathbf{S}_1'$ when the gyrotropic axis is oriented arbitrarily with respect to the interface (the previously mentioned mode coupling does not occur if the diagram for region 1 has the simple shape shown in fig. 9). The configuration in figure 9 may also support a lateral ray. The saddle point condition derived from the exponents in (24) has the general form (23) (when $k_{xs}=0$) and is therefore amenable to the same ray-optical interpretation as in figure 5 (see right-hand side of fig. 9), provided that the ray trajectories and the relations between the angles of incidence, reflection and refraction are those consistent with the refractive index plot. The same comment applies to the ray-optical determination of the final asymptotic field solution, with the detailed behavior of the ray amplitudes inferred again from the appropriate amplitude factor in the integrand.

The remarks in section 4.2d concerning various types of source configurations are pertinent as well for the present discussion. To assess the influence of the boundary on the radiated field, one obtains first the ray configuration in the unbounded medium and then employs the refractive index plots to

trace the progress of the reflected and refracted rays. The observations in section 4.3 are also applicable here.

To illustrate the variety of wave phenomena possible when mode coupling takes place at the boundary, we consider the medium schematized in figure 1, with the gyrotropic axis perpendicular to the interface (see fig. 10). The branches "o" and "e" describe the propagation characteristics of the ordinary and extraordinary waves, respectively, and the circular contour represents the exterior dielectric. Since the diagram is rotationally symmetric about the k_z-axis, the horizontal axis has been labeled k_t. An upgoing (incident) ordinary ray A gives rise to an ordinary reflected ray C, an extraordinary reflected ray D and a refracted ray E; conversely, an incident extraordinary ray B produces a reflected extraordinary ray D, an ordinary ray C and also a refracted ray E, all of which correspond to the same value of k_{ti}. One observes that the incident ordinary and extraordinary rays proceed to entirely different regions of space although both are characterized by a common value of k_{ti}. Moreover, ray E is refracted on the *same* side of the surface normal as the incident ray B, a behavior quite different from that in an isotropic region (backward refraction); backward reflection occurs for rays B, C and A, D.

The possible lateral ray trajectories are particularly interesting. It is seen from figure 10b that an ordinary lateral ray C_1 may be excited by an extraordinary incident ray B_1 and refracted into the extraordinary ray D_1 as well as the exterior ray E_1. This lateral ray travels *inside* the medium containing the source and therefore represents an effect which is not encountered in isotropic problems.[3] In addition, there exists the more conventional lateral ray E_2 which travels in the *exterior* medium [see Felsen, 1963; Tyras, Ishimaru, and Swarm, 1963], is excited by the incident ray B_2 and refracted back into ray D_2. Analytically, the points of emergence of rays C_1 and E_2 on the refractive index diagrams, represent branch points which may be crossed during the asymptotic evaluation of the radiation integrals [see Arbel and Felsen, 1963, for a classification of these singularities]. While the lateral ray amplitude is generally smaller than that on a reflected ray, it is important to note that the lateral rays may sometimes penetrate regions which are inaccessible to the reflected rays, under which circumstances they constitute the dominant contribution. For example, if the anisotropic medium is characterized *only* by the open-branched surface in figure 10 (see also fig. 8), the incident and reflected rays are confined to a limited conical region surrounding the z-axis, whereas no such restriction applies to the lateral ray trajectory $B_2E_2D_2$.

b. Focusing Effects

Anisotropy in a homogeneous medium may produce focusing of the energy radiated by a confined

---

[3] Similar phenomena occur in radiation problems involving elastic media [see Ewing, Jardetzky, and Press, 1957].
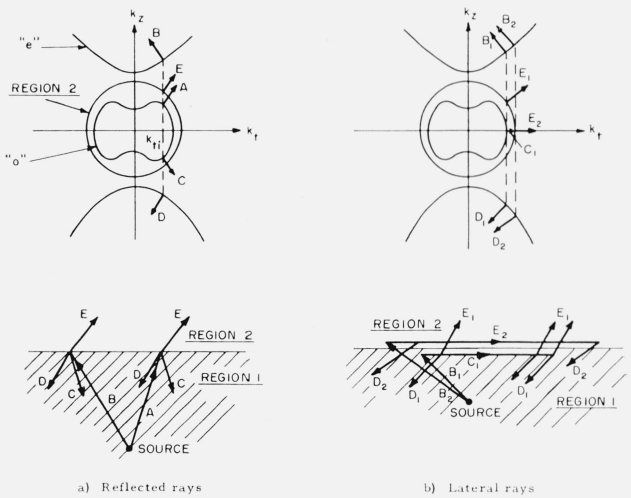

a) Reflected rays   b) Lateral rays

FIGURE 10. *Ray configurations.*

a. Reflected rays.
b. Lateral rays.

source distribution, thereby providing another class of phenomena not observed in isotropic regions. It has already been noted in section 3.3 that certain features in the refractive index diagram (undulations or open branches) may lead to field enhancements along certain directions in an infinite medium. In addition, focusing may occur due to the presence of a plane interface [Felsen, 1964b]. This may be understood from analytical considerations by recalling that the asymptotic evaluation of the radiation integrals leads to an amplitude dependence which is essentially proportional to $P=(d^2\varphi/dk_y^2)_s^{-1/2}$, where φ is one of the exponents in (24) and the evaluation is made at the saddle point k_{ys}. (For simplicity, we consider only the case $k_x \equiv 0$ appropriate, for example, to line source excitation.) Since

$$\frac{d^2\varphi}{dk_y^2}=\frac{d^2k_{zi}^{(o,e)}}{dk_y^2}|z|+\frac{d^2k_{zi}^{(o,e)}}{dk_y^2}|z'|, \qquad i=1, 2, \quad (25)$$

one observes that P may tend to zero for certain values of $|z|$ when the coefficients multiplying $|z|$ and $|z'|$ have opposite algebraic signs. These coefficients are proportional to the curvature of the refractive index plot and if two separate diagrams or branches with opposite curvature are involved, field enhancement (focusing) due to $P \rightarrow 0$ is possible. This situation occurs, for example, with respect to the circular trace in figure 10 and with the "e" branch as well as the portions of the "o" branch near the k_z-axis, respectively (see also fig. 9). Also, the "o"-trace near the k_t-axis has a curvature opposite to that of the "e" branch. Geometrically, the opposite curvatures imply a crossing of the associated ray family as, for example, of the refracted rays in region 2 of figure 9. Similar crossings occur among the reflected rays C (or D) excited by incident rays B (or A), as one may easily ascertain from the refractive index diagram. When two closely adjacent rays of the same family intersect, the cross

section of the corresponding ray tube vanishes and the field intensity diverges. While this divergence is only apparent and may be removed by a more careful asymptotic analysis [Felsen, 1964b], it locates those regions where focusing takes place.

As an illustration, consider an anisotropic half-space characterized only by the open-branched diagram in figure 10, with the circular contour representing the remaining isotropic region. The refracted ray family, when the source is situated in the anisotropic medium, then takes the form in figure 11a (only one half of the picture is shown). The ray family is bounded by a caustic, two branches of which intersect in a focus on the z-axis. Focusing in the anisotropic region occurs when the source is in the isotropic medium, but the caustic now has the shape sketched in figure 11b.
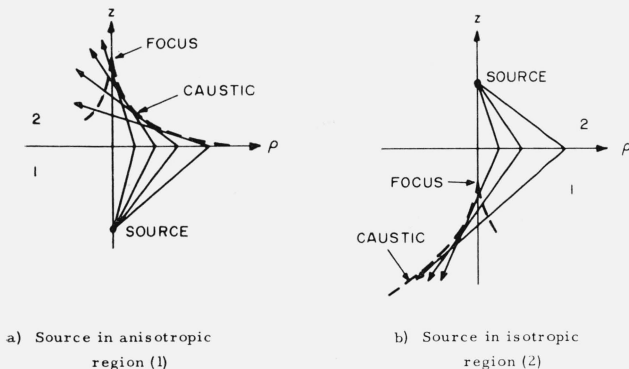

a) Source in anisotropic region (1)

b) Source in isotropic region (2)

FIGURE 11. *Focusing effects due to a plane interface.*
a. Source in anisotropic region (1).
b. Source in isotropic region (2).

6. Summary

It has been shown how the plane wave refractive index diagrams for an infinite anisotropic medium may be employed to predict salient features of the radiation produced by confined source distributions in unbounded or bounded regions. The procedure is essentially one of ray tracing whereby one determines first the rays excited by the given source configuration in an unbounded region, and then accounts for subsequent deviations in trajectories or for generation of new species at a boundary or inhomogeneity. The total field at a given point is comprised of the sum of the fields carried along various rays passing through this point. While the refractive index diagram furnishes direct and general information about the multiplicity of rays excited by point, line, or plane wave sources, detailed features of the ray amplitudes are based on a further knowledge of the source type (electric or magnetic current) and polarization. However, the diagrams reveal easily the existence of spatial regions wherein certain ray amplitudes become very large, thus making possible the prediction of peaks in the radiation pattern. They also permit the determination of caustic and focal areas arising from mode conversion or refraction at an interface, thereby locating other regions of space characterized by enhanced field strengths. The validity of these concepts has been illustrated by an appropriate interpretation of various analytical solutions.

The concepts presented here are basic for the construction of a general ray theory in anisotropic media by which one may derive quantitative results for radiation and scattering problems under quite general conditions. Such a theory has been successful in isotropic environments [Keller, 1958] and its extension to the anisotropic case is aided substantially by the considerations described in this paper. Some results have already been obtained [Felsen, 1963, 1964 a, b; Rulf and Felsen, 1964] and further work in this area is in progress.

7. References

Abraham, L. G., Jr. (1953), Extensions of the magneto-ionic theory to radio wave propagation in the ionosphere, including antenna radiation and plane wave scattering, Report No. 13 (School of Engineering, Cornell Univ., Ithaca, N.Y.).

Allis, W. P. (1961), Propagation of waves in a plasma in a magnetic field, IRE Trans. Microwave Theory Tech. **MTT–9**, No. 1, 79–82.

Allis, W. P., S. J. Buchsbaum, and A. Bers (1962), Waves in plasmas (John Wiley and Sons, New York, N.Y.).

Arbel, E., and L. Felsen (1963), Theory of radiation from sources in anisotropic media. Part I. General sources in stratified media. Part II. Point source in infinite, homogeneous medium, Electromagnetic Waves, ed. E. C. Jordan, 391–459 (Pergamon Press, New York, N.Y.).

Barsukov, K. A. (1959), Radiation of electromagnetic waves from a point source in a gyrotropic medium with a separation boundary, Radiotekh, i elektronica **4**, No. 11, 1759–1764.

Brekhovskikh, L. M. (1960), Waves in layered media, section 21 (Academic Press, New York, N.Y.).

Budden, K. G. (1961), Radio waves in the ionosphere, sections 13.3; 13.18; 13.21 (Cambridge University Press, Cambridge, Eng.).

Clemmow, P. C. (1963), On the theory of radiation from a source in a magneto-ionic medium, Electromagnetic Waves, ed. E. C. Jordan, 461 (Pergamon Press, New York, N. Y.).

Clemmow, P. C., and F. Mullaly (1955), The dependence of the refractive index in magneto-ionic theory on the direction of the wave normal, The Physics of the Ionosphere, 340 (The Physical Society, London, Eng.).

Deschamps, G., and W. L. Weeks (1962), Charts for computing the refractive indexes of a magneto-ionic medium, IRE Trans. Ant. Prop. **AP–10**, 305–317.

Ewing, W. M., W. S. Jardetzky, and F. Press (1957), Elastic waves in layered media, section 3.3 (McGraw-Hill Book Co., New York, N.Y.).

Felsen, L. B. (1963), Radiation from a uniaxially anisotropic plasma half-space, IEEE Trans. Ant. Prop. **AP–11**, 469–484.

Felsen, L. B. (1964a), Propagation and diffraction in uniaxially anisotropic regions. Part. I. Theory. Part II. Applications, Proc. IEE (London) **111**, No. 3, 445–464.

Felsen, L. B. (1964b), Focusing by an anisotropic plasma interface, IEEE Trans. Ant. Prop. **AP–12**, 624–635.

Felsen, L. B., and B. Rulf (Aug. 1963), Radiation from a directive antenna embedded in an anisotropic half-space, Report PIBMRI–1183–63 (Electrophys. Dept., Polytechnic Institute of Brooklyn, Brooklyn, N.Y.).

Ginzburg, V. L. (1960), Propagation of electromagnetic waves in plasma, section 24 (Gordon and Breach, Science Publishers, Inc., New York, N.Y.).

Hines, C. O. (1951), Wave packets, the Poynting vector and energy flow. Part I: non-dissipative (anisotropic) homogeneous media, J. Geophys. Res. **56,** 63.

Keller, J. B. (1958), A geometrical theory of diffraction, in Calculus of variations and its applications (McGraw-Hill Book Co., New York, N.Y.).

Kogelnik, H., and H. Motz (1963), Electromagnetic radiation from sources embedded in an infinite anisotropic medium and the significance of the Poynting vector, Electromagnetic Waves, ed. E. C. Jordan, 477 (Pergamon Press, New York, N.Y.).

Lighthill, M. J. (1960), Studies on magneto-hydrodynamic waves and other anisotropic wave motions, Phil. Trans. Roy. Soc. London **252,** Ser. A, 397–430.

McKenzie, J. F. (1963), Cerenkov radiation in a magneto-ionic medium, Phil. Trans. Roy. Soc. London **255,** Ser. A, 585–606.

Mittra, R., and G. A. Deschamps (1963), Field solution for a dipole in an anisotropic medium, Electromagnetic Waves, ed. E. C. Jordan, 495 (Pergamon Press, New York, N.Y.).

Rulf, B., and L. B. Felsen (1964), Diffraction by objects in anisotropic media, Proceedings of the Symposium on Quasi-Optics, p. 107. (Polytechnic Press, Polytechnic Institute of Brooklyn).

Stix, T. H. (1962), The theory of plasma waves, section 2.3; 3.4 (McGraw-Hill Book Co., New York, N.Y.).

Stratton, J. A. (1941), Electromagnetic theory, section 9.29 (McGraw-Hill Book Co., New York, N.Y.).

Tyras, G., A. Ishimaru, and H. M. Swarm (1963) Lateral waves on air-magneto-plasma interfaces, Electromagnetic waves, ed. E. C. Jordan, 517 (Pergamon Press, New York, N.Y.).